

# A method for enhancing the stability and robustness of explicit schemes in CFD

Hujeirat, A. <sup>1</sup>

*Institute of Applied Mathematics, University of Heidelberg, 69120 Heidelberg, Germany*

---

## Abstract

A method for enhancing the stability and robustness of explicit schemes in computational fluid dynamics is presented. The method is based in reformulating explicit schemes in matrix form, which can then be modified gradually into semi or strongly-implicit schemes.

From the point of view of matrix-algebra, explicit numerical methods are special cases in which the global matrix of coefficients is reduced to the identity matrix  $I$ . This extreme simplification leads to severe limitation of their stability range, hence of their robustness.

In this paper it is shown that a condition, which is similar to the Courant-Friedrich-Levy (CFL) condition can be obtained from the stability requirement of inversion of the coefficient matrix. This condition is shown to be relax-able, and that a class of methods that range from explicit to strongly implicit methods can be constructed, whose degree of implicitness depends on the number of coefficients used in constructing the corresponding coefficient-matrices. Special attention is given to a simple and tractable semi-explicit method, which is obtained by modifying the coefficient matrix from the identity matrix  $I$  into a diagonal-matrix  $D$ . This method is shown to be stable, robust and it can be applied to search for stationary solutions using large CFL-numbers, though it converges slower than its implicit counterpart. Moreover, the method can be applied to follow the evolution of strongly time-dependent flows, though it is not as efficient as normal explicit methods.

In addition, we find that the residual smoothing method accelerates convergence toward steady state solutions considerably and improves the efficiency of the solution procedure.

*Key words:* Numerical Methods, Hydrodynamics, Astrophysical Fluid Dynamics

*PACS:* 02.60, 95.30.L, 95.30.Q, 47.70

---

<sup>1</sup> E-mail: ahmad.hujeirat@iwr.uni-heidelberg.de

## 1 Introduction

In the last two decades, tremendous progress has been made in both computational fluid dynamics (CFD) algorithms and the computer hardware technologies. The computing speed and memory capacity of computers have increased exponentially during this period. Similarly is astrophysical fluid dynamics (AFD), which is considered nowadays as a rapidly growing research field, in which modern numerical methods are extensively used to model the evolution of rather complicated flows. Unlike CFD, in which implicit methods are frequently used, the majority of the methods used in AFD are explicit. Several of them became very popular, e.g., ZEUS (Stone & Norman 1992), NIRVANA+ (Ziegler 1998), FLASH (Fryxell et al. 2000), VAC (Tóth et al. 1998), THARM (Gammie et al. 2003). The popularity of explicit methods arises from their being easy to construct, vectorizable, parallelizable and even more efficient as long as the dynamical evolution of compressible flows is concerned. Specifically, for modeling the dynamical evolution of HD-flows in two and three dimensions explicit methods are highly superior to-date. For modelling relativistic flows, Koide and collaborators (e.g., Koide et al. 2000, 2002, Meier et al. 2001) and Komissarov (2001) have developed pioneering general relativistic MHD solvers. A rather complete review of numerical approaches to relativistic fluid dynamics is given by Martí & Müller (1999) and Font (2000). A ZEUS-like scheme for general relativistic MHD has also been developed and is described in De Villiers & Hawley (2003).

However, these methods are numerically stable as far as the Courant-Friedrich-Levy number is smaller than unity. The corresponding time step size decreases dramatically with the incorporation of real astrophysical effects. Specifically, they may even stagnate if self-gravity, radiative and chemical effects are included. Moreover, explicit methods break down if the flow is weakly or strongly incompressible, and if the domain of calculations is subdivided into a strongly stretched mesh. In an attempt to enhance their robustness, several alternatives have been suggested, such as semi-explicit, semi-implicit or even implicit-explicit methods (Kley 1989, Tóth et al. 1998). Nevertheless, their rather limited range of applications has led to the fact that most of the interesting astrophysical problems remained, indeed, not really solved. A simple example is the evolution of a steady turbulent accretion disk. It was found by Balbus & Hawley (1991) that weak magnetic fields in accretion disks are amplified, generate turbulence, which in turn redistribute the angular momentum in the disk. However, whether this instability leads to the long-sought global steady accretion rate, or is it just a transient phenomenon in which the generation of turbulence is subsequently suppressed by dynamo action are not at all clear. Other notable phenomena are the formation and acceleration of the observed superluminal jets in quasars and in microquasars, the origin of the quasi-periodic oscillation in low mass X-ray binaries or the progenitors of gamma ray burst are still spectacular.

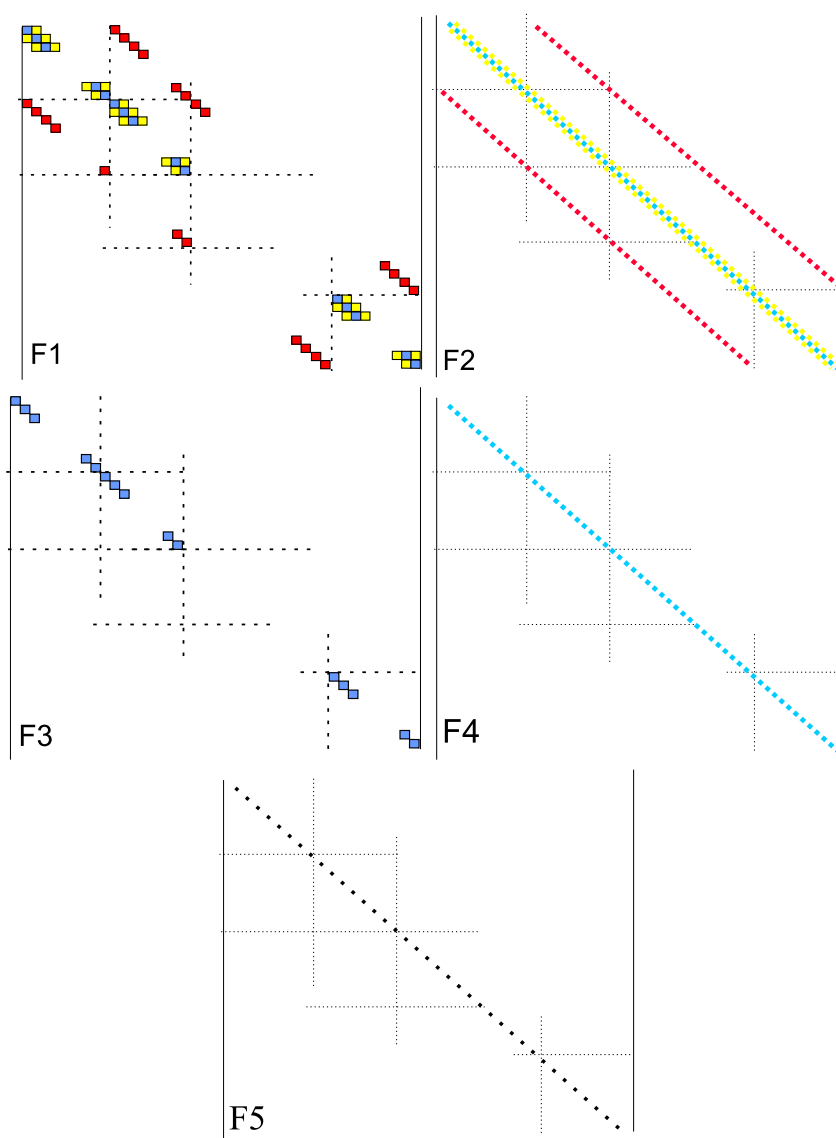


Fig. 1. Schematic description of several coefficient matrices used by different numerical solution procedures in two dimensions. Most commonly used matrices are F1, F2, F3, F4 and F5, which correspond to tri-diagonal block, scalar tri-diagonal, block diagonal, scalar diagonal and identity matrices, respectively. Solution methods that rely on the inversion of F1 are classified as implicit, whereas those relying on F5 are explicit. F2, F3 and F3 correspond to intermediate methods, i.e., explicit-implicit methods.

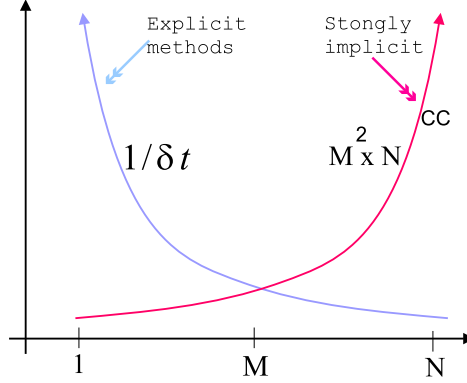


Fig. 2. A schematic description of the time step size and the computational costs versus the band width  $M$  of the coefficient matrix.  $N$  is the number of unknowns. Explicit methods correspond to  $M = 1$  and large  $1/\delta t$ . They require minimum computational costs (CC). Large time steps (i.e., small  $1/\delta t$ ) can be achieved using strongly implicit methods. These methods generally rely on the inversion of matrices with large band width, hence computationally expensive, and, in most cases, are inefficient.

Explicit methods rely on time-extrapolation procedures for advancing the solution in time. However, in order to provide physically consistent solutions, it is necessary that these procedures are numerically stable. The usual approach for examining the stability of numerical methods is to perform the so called von Neumann analysis (see Hirsch 1988 for further details). For example, using an explicit procedure to solve the simple advection-diffusion equation:

$$T_{,t} + uT_{,x} = \nu T_{,xx} + f, \quad (1)$$

and applying the von Neumann stability analysis, it is necessary, but not sufficient, that the CFL-number is less than unity. This is equivalent to require that the time step size fulfills the inequality:  $\delta t \leq \min(\frac{\Delta X}{|u| + |\frac{\partial f}{\partial \rho}|^{1/2}}, \frac{\Delta X^2}{\nu})$ , where  $T$ ,  $\nu$ ,  $f$ ,  $\rho$  denote an arbitrary diffusible variable, viscosity coefficient, internal or external forces and density of matter, respectively. The sub-scripts  $t$ ,  $x$ ,  $xx$  represent first and second order derivatives of  $T$  with respect to time and to the  $x$ -coordinate. The minimum function in the last inequality runs over each grid point of the domain of calculation. For additional details see Sec. 9.4 in Fletcher (1991). The force  $f$  may corresponds to internal forces, such as thermal, radiative or magnetic pressure. In regions where the density is low (e.g., corona around compact objects such as black holes or even above accretion disks), the derivative  $|\frac{\partial f}{\partial \rho}|^{1/2}$  corresponds to the sound speed, speed of light or to the propagational speed of magnetic Alfvén waves, all of which can be extremely large compared to the actual velocity of the flow. Consequently, the CFL-condition limits the range of application and severely affects the robustness of explicit methods. In particular, equations corresponding to physical processes occurring on much shorter time scales than the hydro-time scale

(e.g., radiation, self-gravitation and chemical reactions) cannot be followed explicitly. Furthermore, these methods are not suited for searching solutions that correspond to evolutionary phases occurring on time scales much longer than the hydro-time scale. Using high performance computers to perform a large number of explicit time steps may lead to accumulation of round-off errors that can easily distort the propagation of information from the boundaries and cause divergence of the solution procedure, especially if Neumann type conditions are imposed at the boundaries.

In contrast to explicit methods, implicit methods are based on solving a matrix equation of the form  $\overline{A}\delta q = d$ , where  $\overline{A}$  is the coefficient matrix resulting from the linearization of the system of equations to be solved,  $d$  is the right hand side vector of known quantities, and  $\delta q$  is the solution vector sought. These methods have two major drawbacks. First, constructing the matrix  $A$  is difficult, time consuming, and may considerably influence the stability and robustness of the method. Second, the inversion procedure must be stable and extremely efficient. In general, conservative discretization of the MHD equations give rise to sparse matrices, or even to narrow band matrices. Therefore, any efficient matrix inversion procedure must take the advantage of  $A$  being sparse (see Fig. 1). Inverting  $A$  directly by using Gaussian elimination requires  $N^3$  algebraic operations, where  $N$  is the number of unknowns (Fig. 2). If the flow is multi-dimensional and a high spatial resolution is required, the number of operations can be prohibitive even on modern supercomputers. Krylov sub-iterative methods (KSIMs), on the other hand, are most suited for sparse matrices and avoid the fill-in procedure. In the latter case,  $A$  is not directly involved in the process, but rather its multiplication with a vector. The convergence rate of KSIMs has been found to depend strongly on the proper choice of the pre-conditioner. For advection-dominated flows, incomplete factorization such as ILU, IC and LQ, approximate factorization, ADI, line Gauss-Seidel are only a small sub-set of possible sequential pre-conditioners (see Saad & van der Vorst 2000 and the references therein). Another powerful way of accelerating relaxation techniques is to use the multi-grid method as direct solver or as pre-conditioner (see Brandt 2001; Trottenberg et al. 2001). For parallel computations, Red-Black ordering in combination with GRMES and Bi-CGSTAB as well as domain decomposition are among the popular pre-conditioners (see Dongarra et al. 1998 for further discussion).

In this paper we present a strategy for enhancing the stability and robustness of explicit methods.

In Sec.2 of this paper we describe and apply the new strategy to scalar equations in one-dimension, and generalize it to system of equations in Sec. 3. Here it is shown that a class of semi-explicit numerical methods can be easily constructed through reformulating explicit methods in matrix form, which thereafter can be modified. Spacial attention is given to a simple semi-explicit method which can be applied for searching stationary solutions. Although The method is easy to program and stable even when using  $CFL > 1$ , it converges

relatively slowly compared to implicit methods, and therefore further additional acceleration techniques of convergence are still to be found. The results of various test calculations are presented in Sec. 5, followed by the summary and conclusions in Sec. 6.

## 2 Stability of matrix inversion and the CFL connection

In fluid flows, the equation of motion which describes hydrodynamically the time-evolution of a quantity  $q$  in conservation form reads:

$$\frac{\partial q}{\partial t} + Lq\vec{V} = f, \quad (2)$$

where  $\vec{V}$  and  $f$  are spatially varying velocity field and external forces, respectively.  $L$  represents a first and/or second order linear differential operator that describe the advection and diffusion of  $q$ . In the finite space  $\mathfrak{R}$ , we may replace the time derivative of  $q$  by:

$$\frac{\delta q}{\delta t} = \frac{q^{n+1} - q^n}{\delta t}, \quad (3)$$

where  $q^n$  and  $q^{n+1}$  correspond to the actual value of  $q$  at the old and new time, levels, respectively.

An explicit formulation of Eq.3 reads:

$$\frac{\delta q}{\delta t} = [-Lq\vec{V} + f]^n, \quad (4)$$

whereas the corresponding implicit form is:

$$\frac{\delta q}{\delta t} = [-Lq\vec{V} + f]^{n+1}. \quad (5)$$

Combining these two approaches together, we obtain:

$$0 = -\frac{\delta q}{\delta t} + \theta[-Lq\vec{V} + f]^{n+1} + (1 - \theta)[-Lq\vec{V} + f]^n \doteq RHS, \quad (6)$$

where  $\theta(0 \leq \theta \leq 1)$  is a switch on/off parameter.

The spatial operator  $H \doteq [-Lq\vec{V} + f]$  should be computed at each grid point, using a conservative discretization. In this case, the coefficients of the Jacobian matrix can be constructed by computing  $\partial RHS / \partial q^{n+1}$  which we decompose

in  $A \doteq -[\partial H/\partial q]^{n+1}$  and  $I/\delta t$ . Thus, Eq. 6 can be replaced by the matrix-equation:

$$\left(\frac{I}{\delta t} + \theta A\right)\delta q = RHS. \quad (7)$$

As a starting condition in each time step, it is suggested to set  $q^{n+1} = q^n$ . Thus, the scheme degenerates into explicit scheme for  $\theta = 0$  and into iterative implicit for  $\theta = 1$ .

Eq. 7. is a combination of the Newton and the Crank-Nicolson methods (Fletcher 1991; p. 165 and 304). It requires that in each time step the RHS should vanish completely. If steady state or quasi-stationary solutions are sought, then both the RHS as well as  $(q^{n+1} - q^n)/\delta t$  must vanish simultaneously. In the latter case, care should be taken to assure that  $\theta \rightarrow 1$  as  $\delta t \rightarrow \infty$ .

We note that since the LHS and the RHS of Eq. 7 are generally different, a loop of iteration within each time step must be constructed in order to obtain a reasonable value for<sup>2</sup>  $q^{n+1}$ .

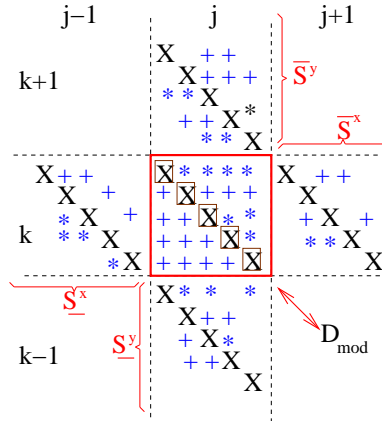


Fig. 3. The neighboring block matrices in the x and y-directions resulting from 5-star staggered grid discretization. Entries marked with ‘X’ denote the elements usually used in the implicit operator splitting approach (Hujeirat & Rannacher 2001), ‘\*’ and ‘+’ are coefficients corresponding to the source terms. The semi-explicit method for a scalar equation relies on inverting the diagonal matrix whose entries are marked with X surrounded by squares. The generalization of the semi-explicit method to the multi-dimensional HD-equations requires inverting the block diagonal matrix  $D_{\text{mod}}$ .

The matrix  $A$  contains coefficients such as  $V/\Delta x$ ,  $\eta/\Delta x^2$  that correspond to advection and diffusion terms, respectively, as well as additional coefficients that correspond to source terms.

<sup>2</sup> Such deviations may evolve if the LHS of Eq. 7 is not precisely the real Jacobian of Eq. 6, and if the equations to be solved are partially non-linear .

Noting that Eq. 2 describes the time evolution of a real physical variable  $q$ , and applying a conservative discretization to the advection operator  $L$ , e.g., first order up-winding, it is easy to verify that the resulting matrix  $\bar{A} = I + \delta t \theta A$  is positive definite (nonsingular) and, diagonally dominant. Therefore, the matrix  $\bar{A}$  can be stably inverted (Hackbusch 1994).

In this case the relevant question is: how far can we simplify  $\bar{A}$ , and still able to provide corrections  $\delta q$ , appropriate for convergence ?

Let us replace the real matrix coefficient  $\bar{A}$  by a matrix  $\tilde{A}$ , which is simple and easy to invert. Thus, instead of solving the “difficult” matrix equation  $\bar{A} \delta q = \delta t RHS$ , we solve  $\tilde{A} \tilde{\delta q} = \delta t RHS$ . However, in order to assure that we are dealing with the original problem still, the matrices  $\bar{A}$  and  $\tilde{A}$  must share the essential spectral properties, i.e, the “spectral equivalence” (Golub & Loan 1989; Hackbusch 1994, p. 217). For example in explicit methods  $\tilde{A} = I$ . In order that the matrices  $I$  and  $\bar{A}$  be spectrally equivalent, the sum of the absolute values of the elements in each row of  $\delta t \theta A$  must be smaller than the corresponding diagonal element of  $I$ . This implies that  $2 \theta |V|/\Delta x < 1/\delta t$ . The latter condition is relatively strong, and a weaker condition can be obtained if the flux difference, rather than the flux itself, is considered. In this case, and in the absence of diffusion and external forces, the following inequality holds:

$$|\Delta V q|/\Delta x < |q|/\delta t, \quad (8)$$

where  $q$  may acquire negative and positive values. However, since  $Vq$  is a conservative quantity, we may obtain an upper limit for the flux-difference:

$$|\Delta V q| \leq \max\{(Vq)_{\text{in}}, (Vq)_{\text{out}}\} = |V||q|, \quad (9)$$

where the sub-scripts “in, out” denote the locations of the in- and out-flows through the surfaces of an arbitrary finite volume cell. In writing the last equality, we have omitted these subscripts for simplicity.

Thus, in terms of Eq. 7, neglecting  $\theta A$  is equivalent to require:

$$|\Delta V q|/\Delta x \leq |V||q|/\Delta x < |q|/\delta t. \quad (10)$$

This is equivalent to the outcome of the von Neumann stability analysis (see Richtmyer & Morton 1967), which yielded the well-known condition  $CFL = |V|\delta t/\Delta x < 1$ .

It should be noted, however, that the classical derivation of the CFL conditions relies on the assumption that the velocity  $V$  in Eq. 2 is constant. Practically, the HD-equations are non-linear, and using  $CFL = 1$  does not prevent the exponential growth of the instability. Indeed, most of the explicit

Fig. 4. The evolution of the residual and the CFL-number versus number of iteration for the heat diffusion equation (Eq. 21). In (a) the time step is constructed directly from the residual. Here the diagonal elements, or equivalently the time step size, oscillates around a canonical value that corresponds to  $CFL = 1$ . The matrix inversion is highly unstable and fails to provide a perturbation-free steady solution. In (b) the time step is set to increase gradually from a small value up to a value that corresponds to  $CFL=1.75$ . The residual in this case grows exponentially, which implies that the matrix coefficient cannot be stable-inverted. In (c) the diagonal elements, i.e.,  $I/\delta t$ , are taken to correspond to  $CFL=0.975$ . In this case the matrix has a stable inversion, hence converges, though extremely slow.

methods used in astrophysical fluid dynamics provide stable solutions, if only the  $CFL$ -number is strictly less than unity, and in most cases, a  $CFL \leq 0.6$  is required. The matrix  $A$  can be decomposed as follows:  $A = D + L + U$ , where  $D$  is a matrix that consists of the diagonal elements of  $A$ .  $L$  and  $U$  contain respectively the sub- and super-diagonal entries of  $A$ . Noting that a con-

servative discretization of the advection-diffusion hydrodynamical equations (Navier-Stokes equations) gives rise to a  $D$  which contains positive values, we may reconstruct a modified diagonal matrix  $D_{\text{mod}} = I/\delta t + \theta D$ . In this case, Eq. 7 is equivalent to:

$$[D_{\text{mod}} + \theta(L + U)]\delta q = RHS. \quad (11)$$

A slightly modified semi-explicit form can be obtained by neglecting the entries of the matrix  $\theta(L + U)$ . In this case, a necessary condition for the iteration procedure to converge is that the absolute value of the sum of elements in each row of  $\theta(L + U)$  must be much smaller than the corresponding diagonal element of  $D_{\text{mod}}$  in the same row. In terms of Equation 9, the method is said to converge if the entries in each row of  $D_{\text{mod}}$  fulfill the following condition:

$$1/\delta t + \theta(|V|/\Delta x + \eta/\Delta x^2 + g) > \|A - D\|_{\infty}, \quad (12)$$

where  $\|A - D\|_{\infty}$  denotes the  $\infty$ -norm of  $A - D$ , i.e., the maximum row sum of the modulus of the elements of  $A - D$ . This condition can be fulfilled, however, if the flow is smooth, viscous, and if appropriate boundary conditions are imposed<sup>3</sup>. Consequently, the inversion process of  $D_{\text{mod}}\delta q = RHS$  should proceed stable even when large CFL-numbers are used (see Fig. 6 and 7).

As a numerical test, we have applied this approach to the one-dimensional diffusion equation in spherical geometry (see Eq. 21, see Sec. 5.1, for a detailed description of the physical problem).

In this particular model, the matrix  $A$  of Eq. 7 is removed, and the equation to be solved reads:

$$\left(\frac{I}{\delta t}\right)\delta q = RHS. \quad (13)$$

As a first step, the equation is solved using a direct band matrix solver, where the band width is set to 1. Thus, the solver in this case is exact up to the machine accuracy. The time step size is set to be determined from the residual, without knowing a-priori about the CFL associated-problems. The corresponding results are displayed in Fig. 4. Indeed, we see that the optimal values of the diagonal elements that limit the exponential growth of the residual oscillate around a canonical value which corresponds to CFL=1 (a/ Fig 5). Decreasing the diagonal values artificially, so to correspond to CFL number that is slightly larger than one, gives rise to an exponential growth of the residual (b/ Fig. 4). On the other hand, setting the diagonal values to correspond

---

<sup>3</sup> Note that diffusion pronounces the inequality in Eq. 12, which gives rise to larger CFL-numbers.

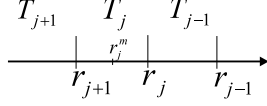


Fig. 5. In the finite volume discretization, the temperature  $T_j$  is defined at the cell center  $r_j^m$ , whose boundaries are  $r_j$   $r_{j+1}$ .

to CFL-numbers that are slightly smaller than unity, we find that the matrix can be stable-inverted, and the resulting solutions converge to the stationary solution, though extremely slowly (c /Fig. 4).

To examine the connection between the stability of the matrix inversion and the CFL condition applied to the heat diffusion equation in  $\mathfrak{R}$ , we may re-write this equation using finite volume discretization (Fig. 5), and use the defect-correction formulation of Eq. 7. Thus, at an arbitrary finite volume cell  $j$ , the equation reads:

$$[\underline{S}_{j-1}]\delta T_{j-1} + [1/\delta t + D_j]\delta T_j + [\overline{S}_{j+1}]\delta T_{j+1} = RHS_j, \quad (14)$$

where  $\underline{S}_{j-1}(= -[\nu/vol_j] \times [r_j^2/\Delta r_j^m])$ ,  $\overline{S}_{j+1}(= -[\nu/vol_j] \times [r_{j+1}^2/\Delta r_{j+1}^m])$ , and  $D_j(= -\underline{S}_{j-1} - \overline{S}_{j+1})$  correspond to the sub-diagonal, super-diagonal and to the diagonal entries of the coefficient matrix. Here  $\Delta r_j^m = (r_{j-1}^m - r_j^m)$ ,  $vol_j = (r_j^3 - r_{j+1}^3)/3$  and  $RHS_j = -(\frac{T^{n+1} - T^n}{\delta t}) + (\frac{\nu}{vol_j})\{r_j^2(\frac{T_{j-1}^i - T_j^i}{\Delta r_j^m}) - r_{j+1}^2(\frac{T_j^i - T_{j+1}^i}{\Delta r_{j+1}^m})\}^{n+1} + 1$ .

Let us consider the following three cases:

- (1) The matrix corresponding to Eq. 14 is diagonally dominant for every time step size  $\delta t$ , hence it can be stable-inverted.
- (2) If we neglect the sub- and super-diagonal entries and preserve  $D_j$ , then the diagonal dominance of the matrix is not affected, maintaining thereby its stability for any time step size  $\delta t$ .
- (3) If we decide, however, to neglect  $D_j$ ,  $\underline{S}_{j-1}$  and  $\overline{S}_{j+1}$ , then it is necessary that  $[1/\delta t]$  be larger than each of the neglected values at every grid point and for all times, i.e.,  $[1/\delta t] > |\underline{S}_{j-1}| + |\overline{S}_{j+1}| \quad \forall j \in (1, N)$ . This is equivalent to require:

$$\delta t < \left(\frac{vol_j}{\nu}\right)\left(\frac{\Delta r_j^m \Delta r_{j+1}^m}{r_j^2 \Delta r_{j+1}^m + r_{j+1}^2 \Delta r_j^m}\right).$$

In plane geometry, this inequality reduces to:

$$\delta t < \left(\frac{\Delta X_j}{\nu}\right)\left(\frac{\Delta X_j \Delta X_{j+1}}{\Delta X_j + \Delta X_{j+1}}\right),$$

which must be fulfilled at every finite volume cell. This inequality is extremely similar to the CFL condition resulting from von Neumann stability analysis.

Therefore, the narrow range of stability of explicit methods is a consequence of over-simplification of the coefficient matrix.

### 3 System of equation - general case

The set of 2D-hydrodynamical equations in conservative form and in Cartesian coordinates may be written in the following vector form:

$$\frac{\partial \vec{q}}{\partial t} + L_{x,xx} \vec{F} + L_{y,yy} \vec{G} = \vec{f}, \quad (15)$$

where  $F$  and  $G$  are fluxes of  $q$ , and  $L_{x,xx}$ ,  $L_{y,yy}$  are first and second order transport operators that describe advection-diffusion of the vector variables  $\vec{q}$  in x and y directions.  $\vec{f}$  corresponds to the vector of source functions.

By analogy with Eq.7, when linearization Eq. 15, the following matrix form can be obtained:

$$\left[ \frac{I}{\delta t} + \theta(AL_{x,xx} + BL_{y,yy} - H) \right] \delta q = RHS, \quad (16)$$

where  $A [= \partial F / \partial q]$ ,  $B [= \partial G / \partial q]$  and  $H [= \partial \vec{f} / \partial q]$ , are evaluated on the former (or the new, if Newton method is used to construct the matrices) time levels.  $RHS^n = [\vec{f} - L_{x,xx} \vec{F} - L_{y,yy} \vec{G}]^n$ .

Adopting a five star staggered grid discretization, it is easy to verify that at each grid point Eq. 16 acquires the following block matrix equation:

$$\begin{aligned} \frac{\delta q_{j,k}}{\delta t} + \underline{S}^x \delta q_{j-1,k} + D^x \delta q_{j,k} + \overline{S}^x \delta q_{j+1,k} \\ + \underline{S}^y \delta q_{j,k-1} + D^y \delta q_{j,k} + \overline{S}^y \delta q_{j,k+1} = RHS_{j,k}, \end{aligned} \quad (17)$$

where the underlines (overlines) mark the sub-diagonal (super-diagonal) block matrices in the corresponding directions (see Fig. 3).  $D^{x,y}$  are the diagonal block matrices resulting from the discretization of the operators  $L_{x,xx} \vec{F}$ ,  $L_{y,yy} \vec{G}$  and  $\vec{f}$ .

To outline the directional dependence of the block matrices, we re-write Eq. 17 in a more compact form:

$$\begin{aligned} \overline{S}^y \delta q_{j,k+1} \\ + \underline{S}^x \delta q_{j-1,k} + D_{\text{mod}} \delta q_{j,k} + \overline{S}^x \delta q_{j+1,k} = RHS_{j,k} \\ + \underline{S}^y \delta q_{j,k-1}. \end{aligned} \quad (18)$$

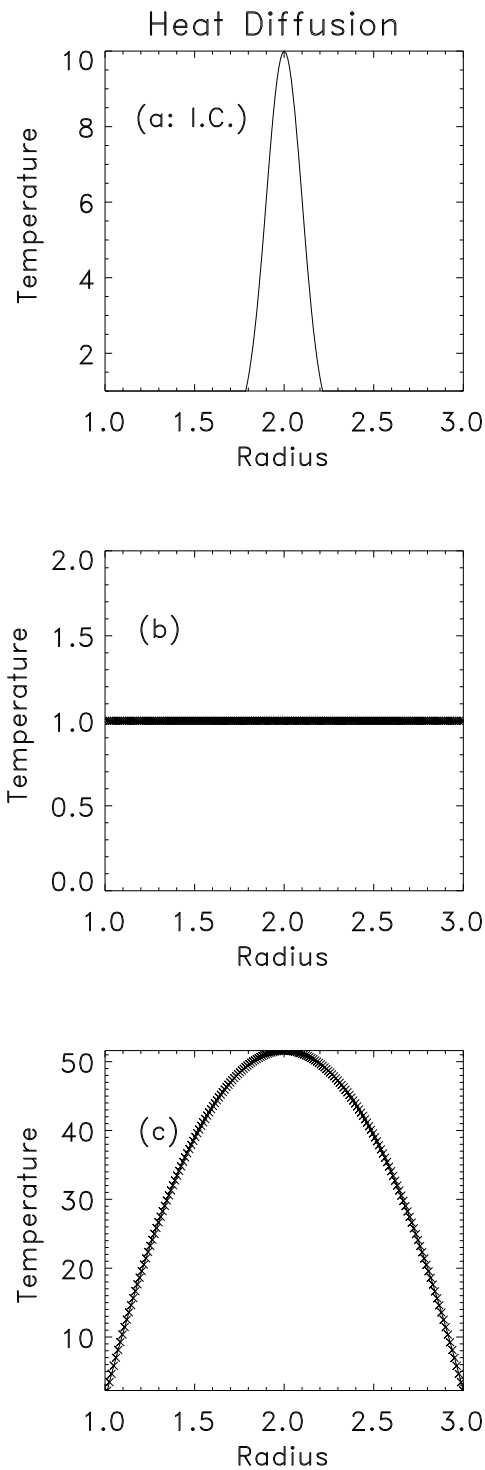


Fig. 6. The one-dimensional heat diffusion problem. The profile in (a) corresponds to the initial distribution of the temperature. The T-profile in (b) is a steady solution which was obtained without a source term, i.e., by solving the equation:  $T_{,t} = r^{-2}(r^2\nu T_{,r})_{,r}$  (see Sec. 5.1). The profile (c) corresponds to the stationary solution obtained with a source term (see Eq. 21).

Fig. 7. The one-dimensional heat diffusion problem. The evolution of the CFL-number ( $\nu \delta t / \Delta x^2$ , solid line) and the residual (dashed line, *RHS* of Eq. 7) versus number of iteration for different numerical methods. While the explicit method stagnates after 130000 time steps, the semi-explicit method converges to the steady solution after 20000 time steps. On the other hand, the fully implicit method provides the sought solution after 100 iterations only. Although in the latter case the defect-correction strategy in combination with several global iterations have been employed to assure convergence, the implicit solution procedure is remarkably more robust and more efficient than the former methods.

where  $D_{\text{mod}} = \delta q_{j,k}/\delta t + D^x + D^y$ . The subscripts “j” and “k” denote the grid-numbering in the x and y directions, respectively (see Fig. 3). Eq. 18 gives rise to three different types of solution procedures:

- (1) Classical explicit methods are obviously very special cases that are recovered when the sub- and super-diagonal block matrices together with  $D^x$  and  $D^y$  are neglected. The only matrix to be retained here is  $(1/\delta t) \times$  (the identity matrix), i.e., the first term on the LHS of Eq. 16. This yields the vector equation:

$$\frac{I}{\delta t} \delta q_{j,k} = RHS_{j,k}. \quad (19)$$

- (2) Semi-explicit methods are recovered when neglecting the sub- and super-diagonal block matrices only, but retaining the block diagonal matrices. In this case the matrix equation reads:

$$D_{\text{mod}} \delta q_{j,k} = RHS_{j,k}. \quad (20)$$

We note that inverting  $D_{\text{mod}}$  is a straightforward procedure, which can be maintained analytically or numerically.

- (3) A fully implicit solution procedure requires retaining all the block matrices on the LHS of Eq. 18. This yields a global matrix that is highly sparse (a/ Fig.1). In this case, the “Approximate Factorization Method” (-AFM: Beam & Warming 1978) and the “Line Gauss-Seidel Relaxation Method” (-LGS: MacCormack 1985) are considered to be efficient solvers for such a set of HD-equations in multi-dimensions.

### 3.1 Residual smoothing and accelerating convergence

Let [a,b] be the interval on which Eq. 2 should to be solved. We may divide [a,b] into N equally spaced finite volume cells:  $\Delta x_i = (b - a)/N$ ,  $i = 1, N$ . To follow the time-evolution of q using a classical explicit method, the time step size must fulfill the CFL-condition, which requires  $\delta t$  to be smaller than the critical value:  $\delta t_c^u$ . If [a,b] is divided into N highly stretched finite volume cells, for example  $\Delta x_1 < \Delta x_2 \dots < \Delta x_N$ , then the CFL-condition restricts the time step size to be even smaller than  $\delta t_c^m = \min_i \{(\Delta x_i / (V + V_S))_i\}$ , which is much smaller than  $\delta t_c^u$ . Thus, applying a conditionally stable method to model flows, while using a highly non-uniform distributed mesh, has the disadvantage that the time evolution of the variables in the whole domain are artificially and severely affected by the flow behaviour on the finest cell.

Moreover, time-advancing the variables may stagnate if the flow is strongly or nearly incompressible. In this case,  $V_S \gg V$ , which implies that the time step size allowed by the CFL-condition approaches zero.

However, we may still associate a time step size with each grid point, e.g.,  $\delta t_i^{\text{nu}} = \Delta x_i / (V + V_S)$ , and follow the time evolution of variable  $q$  in each cell independently. Interactions between variables enter the solution procedure through the evaluation of the spatial operators on the former time level. This method, which is occasionally called the ‘‘Residual Smoothing Method’’ proved to be efficient at providing quasi-stationary solutions within a reasonable number of iterations, when compared to normal explicit methods (Fig. 10, 13, also see Swanson & Turkel 1997; Enander 1997).

The main disadvantage of this method is its inability to provide physically meaningful time scales for features that possess quasi-stationary behaviour. Here we suggest to use the obtained quasi-stationary solutions as initial configuration and re-start the calculations using a uniform and physically relevant time step size.

#### 4 Other similar approaches

The Dufort-Frankel scheme is most suited for modelling diffusion-dominated flows and provides solutions of second order spatial and temporal accuracies (see Fletcher 1991 for further details). The scheme is unconditionally stable, as it relies on adding the positive coefficient resulting from finite difference discretization of the diffusion operator to the diagonal elements, thereby enhancing the diagonal dominance of the matrix coefficient.

Despite this similarity, the scheme differs still from the explicit-implicit methods presented here at least in two aspects:

- (1) The DuFort-Frankel scheme is generically second order accurate in time. The scheme fails to be consistent when a large time steps are used. Thus, the method is not suited for searching steady state solutions.
- (2) The scheme is not suited for modelling advection-dominated flows.

Another solution procedure that might look similar to the semi-explicit method presented here is the Jacobi iteration method. Inspection of Eq. 20, however, shows that neither the lower nor the upper diagonal matrices are considered in the present solution scheme. Furthermore, the consistency of our solution procedure with the original set of equations is guaranteed through adopting the defect-correction strategy. Unlike Jacobi method which may diverge if large time steps are used, the test calculations presented here show that the semi-explicit method converges even for relatively large CFL numbers.

Recently, Yabe et al. (2001) have presented the Constrained Interpolation Profile (CIP) method, which has been successfully applied to model solid, liquid, gas and plasmas. The method is a kind of semi-Lagrangian scheme which can re-produce strongly time-dependent solutions with large CFL-numbers.

Fig. 8. The wave propagation problem. The initial density profile is the sinus wave (a), which moves right-wards with velocity  $U = 1$ . The computed profiles “b” to “g” have been obtained after time = 1.966, using 200 finite volume cells. The adopted advection scheme is of third order spatial accuracy and second order accurate in time. The profiles “b, d, f” have been obtained using the fully implicit solution procedure with time step sizes that correspond to CFL=1, 2.5 and 5, respectively. The profiles “c, e, g” have been obtained using the semi-explicit approach with CFL=1, 2.5 and 5, respectively.

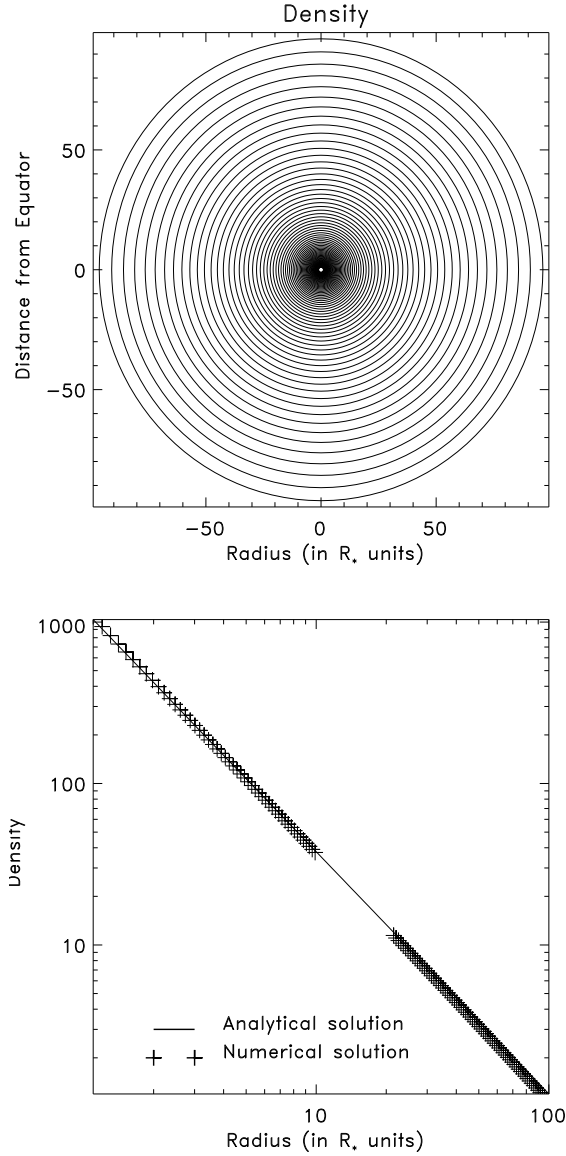


Fig. 9. Free-fall of gas onto a non-rotating black hole. Top: 50 density contours of a freely-falling gas around one solar-mass black hole. Bottom: the numerically-obtained density distribution has a power law that coincides precisely with the theoretical solution  $r^{-3/2}$ . In this calculation, inflow (outflow) at the outer (inner) boundary have been imposed. 200 strongly-stretched finite volume cells in the radial direction and 60 in horizontal direction have been used.

Therefore, the method is promising and testing its robustness and capability at modelling astrophysical phenomena is extremely useful.

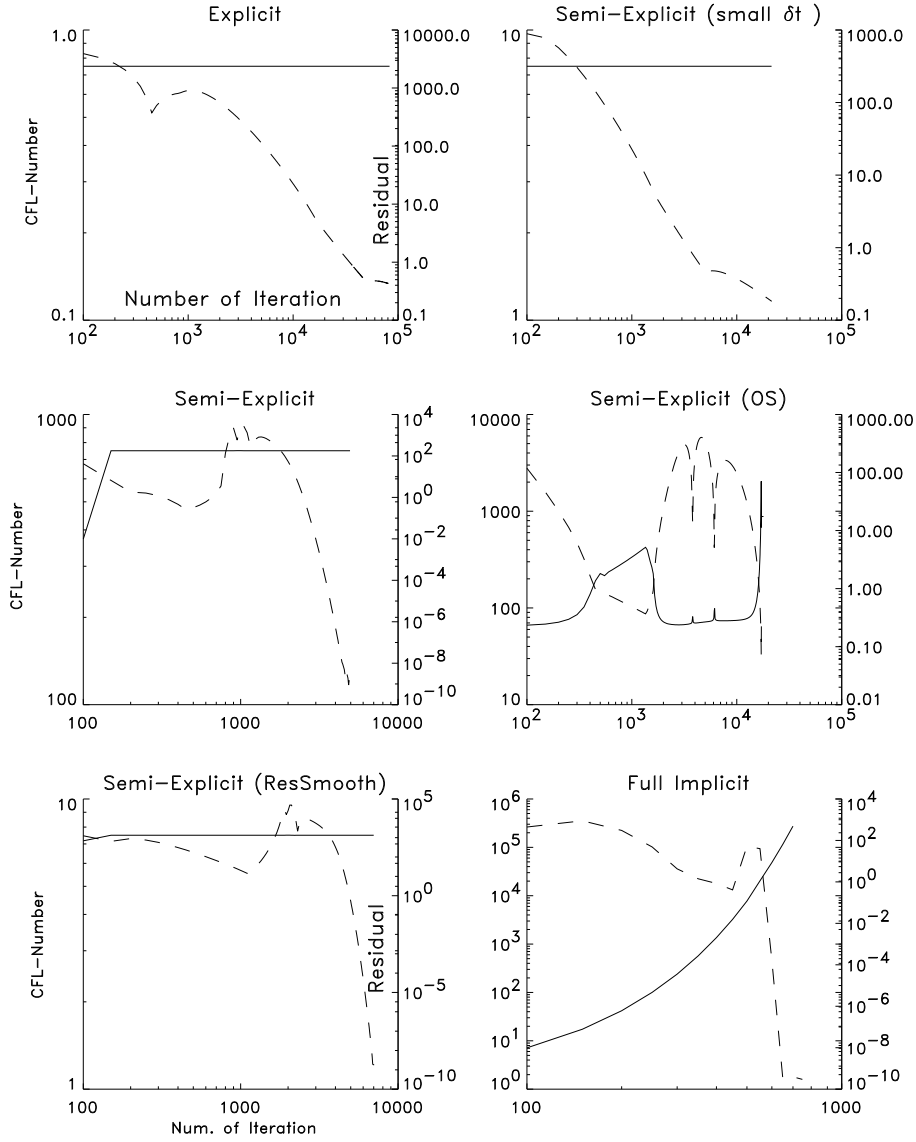


Fig. 10. Plasma in Free-fall onto a black hole. Similar to Fig. 7, the evolution of the CFL-number and the residual versus number of iteration are shown. The solution methods used here are: normal explicit (top/left), semi-explicit (middle/left), semi-explicit in combination with the residual smoothing strategy (bottom/left), semi-explicit using moderate CFL-numbers (top/right), semi-explicit method in which the time step size is taken to be a function of the maximum residual (middle/right), and finally the fully implicit method (bottom/right). Obviously, the different forms of the semi-explicit method used here are stable and converges to the stationary solution, though at different rates.

## 5 Test calculations

In the following, we present the results of several test calculations aimed to examine the stability, robustness and the capability of the semi-explicit solver to treat strongly time-dependent or steady inviscid flows governed by strong shocks.

### 5.1 *The diffusion equation*

Diffusion of heat is generally expressed by a second order differential operator. Taking into account this operator in the von Neumann stability analysis, it can be shown that it imposes a further limitation on the time step size, hence narrowing the stability regime of explicit methods even further. Since this limitation may easily lead to complete stagnation of these methods, especially when steady state solutions are sought, several modification strategies have been suggested. A popular strategy is to treat the diffusion operators implicitly. In the absence of advection and other source terms, however, this modification is significant, as the scheme is then fully implicit, and therefore have the usual drawbacks of implicit methods.

The semi-explicit method presented here is almost as efficient as normal explicit methods. The main difference between these two approaches is that semi-explicit methods require additional programming efforts. Specifically, the positive entries resulting from finite differencing of the operators involved should be carefully selected and added to the diagonal elements of the coefficient matrix.

The purpose here is to apply the semi-explicit method to the heat diffusion problem and compare its convergence behaviour with those of explicit and fully implicit methods.

Similar to the other test calculations presented in this paper, the solvers here are constructed using routines from the solver package “IRMHD” (Hujeirat & Rannacher 2001). The majority of these routines are designed and programmed in spherical geometry. Therefore, to use them properly, the equations of interest should be reformulated in spherical geometry. Unlike in plane geometry, the main drawback of this procedure are the difficulties associated with constructing relevant analytical solutions in spherical geometry. On the other hand, locating the domain of calculation far from the center, may reduce the difference between these geometries ( $\sim 1/r$ ), and which can be made negligibly small.

Thus, the one-dimensional diffusion equation in spherical geometry reads:

$$\frac{\partial T}{\partial t} = \frac{1}{r^2} \frac{\partial}{\partial r} r^2 \nu \frac{\partial T}{\partial r} + 1, \quad (21)$$

where  $T, \nu$  denote the variable temperature and the constant diffusion coefficient, respectively. This equation is solved in the radial direction in the interval  $[r_{\text{in}}, r_{\text{out}}] = [1000, 1003]$ , which is sub-divided into 180 finite volume cells of equal size. The heat equation is solved using the boundary conditions:  $T(r_{\text{in}}) = T(r_{\text{out}}) = 1$ . Note that the inner and outer boundaries are chosen to be very close in order to reduce geometric compression. Furthermore, to pronounce the difference in the convergence history between the explicit, semi-explicit and fully implicit methods, we set  $\nu = 10^{-2}$  and use an initial configuration that is very different from the sought steady solution. Specifically, the calculations have been initialized using the starting profile:  $T(r, t = 0) = 10 e^{-10(r-r_o)^2}$ , where  $r_o = (r_{\text{in}} + r_{\text{out}})/2$  (see Fig.12). To first order in  $(1/r)$ , the steady solution is very close to:  $T(r, t = \infty) = -\frac{1}{2\nu}(r - r_{\text{in}})(r - r_{\text{in}}) + 1$ .

In Fig. 6 and 7 the results of three different solution procedures are presented. For simplicity, the T-profiles in this figure are plotted versus  $\bar{r} = r - 1000$ . Obviously, the semi-explicit method converges to the sought steady solution much faster than explicit, but extremely slower than the fully implicit solver. Moreover, the method is numerically stable even when extremely large CFL-numbers are used.

## 5.2 Wave propagation in one dimension

In an attempt to examine the capability of the method at capturing strongly time dependent features, the following one-dimensional wave equation in spherical geometry has been solved:

$$\frac{\partial \rho}{\partial t} + \frac{1}{r^2} \frac{\partial}{\partial r} r^2 \rho U = 0, \quad (22)$$

where  $\rho, U$  denote the density and radial velocity, respectively. The velocity assumes the constant value  $U = 1$ . To reduce the effect of geometrical compression, the interval of calculation is taken to be  $[100 \leq r \leq 104]$ . Similar to the previous test problems, different solution procedures have been adopted using advection schemes of third order spatial accuracy and second order accurate in time.

The initial density distribution, is taken to be a sinus profile that moves rightwards with velocity  $U = 1$  ( see Fig. 8, plot a). As in plane geometry, the

shape of the initial density profile is expected to be preserved as it moves right-wards.

To compare results, a reference solution has been produced using an explicit solution procedure. The interval of calculation has been sub-divided into 1000 finite volume cells, and a time step size that corresponds to  $CFL = 0.01$  has been used. The advection scheme here is third order accurate in space and second order in time.

Obviously, the semi-explicit method is capable at capturing the propagation of the wave front accurately (see Fig. 8). The amplitude of the wave is hardly changed, even when using a time step size that corresponds to a CFL-number larger than unity. However, in the latter case, several iterations per time step were required to assure convergence. For example, the profile “e” of Fig. 8 has been obtained using  $CFL = 2.5$  in combination with two global iterations per time step, which apparently are not sufficient for convergence. However, increasing the number of iteration from 2 to 7, a more accurate solutions has been obtained even when the CFL number is increased from 2.5 to 5 (see Fig. 8 /profile “g”). Consequently, convergence can be maintained if a sufficient number of global iterations is performed<sup>4</sup>, though the exact correlation is hard to deduce. We note, however, that the LHS and RHS of Equations 7 or 16 may differ significantly from each other if the flow is strongly time-dependent. Here the RHS is calculated using higher order spatial and temporal accuracies, whereas the LHS is calculated using first order accuracies. Maintaining compatibility, in this case, depends on the number of global iterations performed, which is expected to increase with increasing the CFL-number, but which may diverge if the flow contains discontinuities or shocks.

The profile “f” of Fig. 8 show that even fully implicit methods (without iteration, hence the LHS and RHS are weak compatible) may fail to reproduce the correct wave profile, if large CFL-numbers are used.

According to Eq. 6, using  $\theta < 1$  yields a certain average of the  $q$ -values on the new and old time levels. This averaging-process is useful if the sought solutions are strongly time-dependent, such as propagations of shock waves, where using large time-steps may cause divergence of the solution track, or even numerically-destabilize the scheme. A possible way to capture both time-dependent and quasi-stationary solutions is to relate  $\theta$  to the time step size, which in turns depends on the total residual. An example is the damped Crank-Nicolson scheme:  $\theta = (1 + \alpha \delta t)/2 \leq 1$ , where  $\alpha$  is a constant of order unity (see Hujeriat & Rannacher 2001 and the references therein). In the case that stationary solutions are of interest,  $\theta = 1$  should be used.

---

<sup>4</sup> Using high spatial and temporal accuracies may lead to significant deviations of the LHS from the RHS of Eq. 7. This has the consequence that several iterations might be still required to reduce the RHS to below a certain critical value.

### 5.3 Free-fall onto a black hole

A non-rotating gas around a spinless black hole is gravitationally bound, and therefore should fall-freely onto the black hole, provided that no other forces oppose gravity. The density and velocity profiles of a freely-falling matter in the radial direction and far from the event horizon obey the power laws:  $r^{-3/2}$  and  $r^{-1/2}$ , respectively. This physical problem is relevant for testing the capability of the numerical approach at capturing steady and oscillation-free solutions, even when a strongly stretched mesh distribution is used.

The equations to be solved in this problem are the continuity, the radial and horizontal momentum equations, and the internal energy equation. The flow is inviscid and adiabatic with the adiabatic index  $\gamma = 5/3$ . The equations have been solved using a first order accurate advection scheme both in space and time. In carrying out these calculations, the following conditions/inputs have been taken into account.

- The central object is a one solar-mass non-rotating black hole.
- The outer boundary is 100 times larger than the the inner radius, i.e.,  $R_{\text{out}} = 100 \times R_{\text{in}}$ , where  $R_{\text{in}}$  is taken to be the radius of the last stable orbit<sup>5</sup>  $R_{\text{LS}}$ . To first order in  $V/c$ , the flow at this radius can be still treated as non-relativistic, though the error can be as large as 30%.
- Along the outer boundary, the density and temperature of the gas assume uniform distributions, and flow across this boundary with the free-fall velocity. Symmetry boundary conditions along the equator, and asymmetry boundary conditions along the axis of rotation have been imposed. Along the inner boundary, we have imposed non-reflecting and outflow conditions. This means that up-stream conditions are imposed, which forbid information exterior to the boundary to penetrate into the domain of calculations. In particular, the actual values of the density, temperature and momentum in the ghost zone  $r$  are erased and replaced by the corresponding values in the last zone, i.e, the zone between  $R_{\text{in}}$  and  $R_{\text{in}} + \Delta R$ . In the case that second order viscous operators are considered, care has been taken to assure that their first order derivatives across  $R_{\text{in}}$  are vanished.

The above set of equations are solved in the first quadrant  $[1 \leq r \leq 100] \times [0 \leq \theta \leq \pi/2]$ , where 200 strongly stretched finite volume cells in the radial direction and 60 in the horizontal direction are used.

Fig. 9 shows the 2D distribution of the density around the hole. The bottom

---

<sup>5</sup>  $R_{\text{LS}} = 3 \times R_{\text{S}} = 6 \times R_{\text{g}}$ , where  $R_{\text{S}}$  and  $R_{\text{g}}$  are the Schwarzschild and gravitational radii, respectively.

plot of Fig. 9 shows the precise agreement of the numerical with the theoretical solution.

As in Fig. 7, we show in Fig. 10 the evolutions of the CFL-number and the residual as function of the number of iteration which has been obtained using different numerical approaches. The results show that the convergence of the explicit and semi-explicit methods are rather slow when a relatively small time step size is used. This implies that the amplitude-limited oscillations are strongly time-dependent that may result from geometric compression. Indeed, these perturbations disappear, when relatively large time-step sizes are used (see Fig. 10, middle/right).

In addition, the semi-explicit solver has been tested in combination with the residual smoothing strategy. As expected, this approach accelerates convergence considerably ( Fig. 10: compare the plots bottom/left with the top/right).

In most of the cases considered here, the time-step size is set to increase in a well-prescribed manner and independent of the residual. However, determining the size of the time step from the residual directly did not provide satisfactory convergence histories (Fig. 10, middle/right).

The results obtained here indicate that the semi-explicit method is stable when compared to normal explicit methods. Furthermore, the semi-explicit method can be applied to search for stationary solutions using large time steps, or equivalently, CFL-numbers that are significantly larger than unity (Fig. 10, middle/left).

#### 5.4 Shock formation around black holes

Similar to the forward facing step in CFD, a cold and dense disk has been placed in the innermost equatorial region:  $[1 \leq r \leq 10] \times [-0.3 \leq \theta \leq 0.3]$ <sup>1</sup>. We use the same parameters, initial and boundary condition use in the previous flow problem. A vanishing in- and out-flow conditions have been imposed at the boundaries of this disk. The gas surrounding the disk is taken to be inviscid, thin, hot and non-rotating. Thus, the flow configuration is similar to the forward facing step problem usually used for test calculations in CFD. The disk here serves as a barrier that forbids the gas from freely falling onto the black hole, and instead, it forms a curved shock front around the cold disk. The purpose of this test is mainly to examine the capability of the method at capturing steady solution governed by strong shocks. In solving the HD-equations (see Sec. 4.1), an advection scheme of third order spatial accuracy and first order accurate in time has been used. The domain of calculation is sub-divided into 200 strongly-stretched finite volume cells in the radial direction and 60 in

---

<sup>1</sup> In applying spherical geometry, the transformation  $\bar{\theta} = \pi/2 - \theta$  has been used. This is useful if further transformation into cylindrical geometry is planned.

Fig. 11. Free-fall of gas onto a black hole surrounded by a cold disk. Top: the density distribution (red: large values, blue: low values, green: intermediate values). Middle: the temperature distribution (red: large values, blue: low values, gray: intermediate values). The curved shock front, where the temperature attains maxima is obvious. Bottom: the distribution of velocity field.

horizontal direction. In Fig. 11 the configuration of the steady distributions of the density, temperature and the velocity field are shown. Similar to the calculation in the previous sections, the results indicate that the semi-explicit method is stable and converges to the sought steady solution even when a CFL-number of order 200 is used (see Fig. 12). However, the method converges relatively slowly compared to the implicit operator splitting approach, where steady solutions have been obtained after one thousand iterations only.

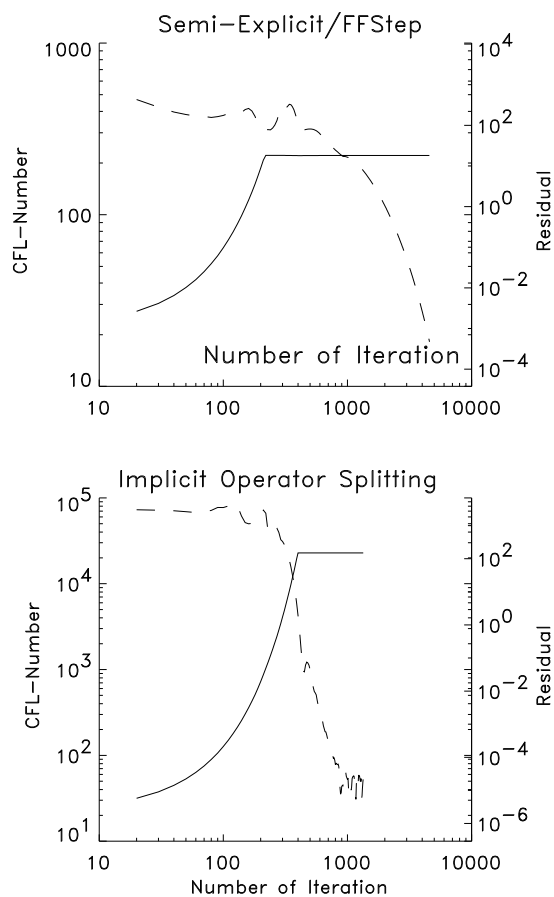


Fig. 12. Free-fall of gas onto a black hole surrounded by a disk. As in Fig. 7, the evolution of the CFL-number and the residual versus number of iteration are shown. The semi-explicit method is apparently stable and converges to the sought stationary solution, even when large time step sizes that corresponds to CFL-number of 220 are used. On the other hand, 1000 iterations were sufficient to obtain the same solution using the implicit operator splitting approach (see Hujeirat & Rannacher 2001).

### 5.5 Weakly incompressible flows between two concentric spheres

To verify the capability of the method at modelling weakly incompressible flows, Taylor flows between two concentric and rotating spheres has been tested (Fig. 14). This is an ideal test problem, as the flow here is viscous (second order diffusive operators are included), closed boundaries (without external perturbations) and the corresponding equations accept strict time-independent solutions.

Fig. 13 shows the time-development of the CFL-number and the total residual for 5-different solution procedures for searching steady state configurations for Taylor flows between two concentric spheres. Using spherical geometry, the set of the 2D axi-symmetric Navier-Stokes equations are solved. The set consists of the three momentum equations, the continuity and the internal energy equations. The flow is assumed to be adiabatic.

As boundary conditions, the inner sphere is set to rotate with  $\Omega = 5$ , whereas the outer sphere has  $\Omega = 0$ . The density, temperature, radial and angular velocities are set to be symmetric along the equator and along the polar axis, except the angular velocity which assumes anti-symmetric conditions along the axis of rotation. For the horizontal velocity, anti-symmetric conditions are imposed both along the equator and along the axis of rotation. On the inner and outer radius of the spheres, all velocity-components are set to vanish. Initially, the flow between the two spheres has zero poloidal and toroidal velocities, so that the rotational energy is injected into the flow through viscous interaction with the inner boundary. In these test calculations, the viscosity coefficient  $\eta = 10^{-2}$  and the switch on/off parameter  $\theta = 1$  have been used. In the explicit case, the equations are solved according to Eq. 19. For the semi-explicit procedure, we solve the HD-equations using the block matrix formulation as described in Equation 20. The implicit operator splitting approach is based in solving each of the HD-equations implicitly. Here, the LGS method has been used in the inversion procedure of each equation (Hujeirat & Rannacher 2001). Unfortunately, while this method has been proven to be robust for modeling compressible flows with open boundaries, it fails to achieve large CFL-numbers in weakly incompressible flows (Fig. 13). This indicates that pressure gradients in weakly incompressible flows do not admit splitting, and therefore they should be included in the solution procedure simultaneously at the new time level.

Using the semi-explicit solution procedure, the CFL-numbers obtained in the present modelling of Taylor flows are, indeed, larger than unity (middle, Fig. 13), but they are not impressively large as we have predicted theoretically. We may attribute this inconsistency to three different effects: 1) The flow considered here is weakly incompressible. This means that the acoustic perturbations have the largest propagational speeds, which require that all pressure effects should be included in the solution procedure simultaneously on the new time

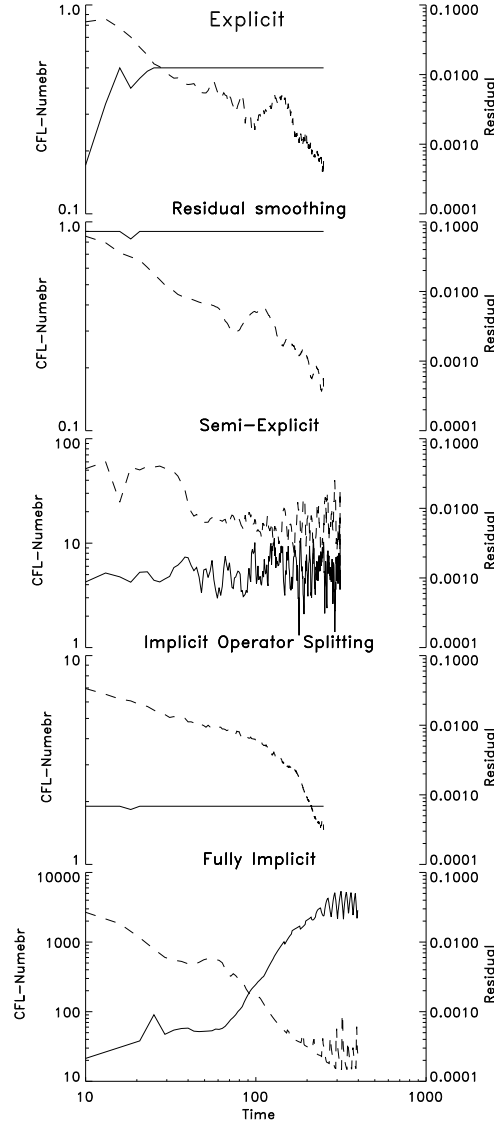


Fig. 13. The development of the CFL-number (left axis, solid line) and the total residual (right axis, dashed line) versus covered-time in normalized units of five different numerical methods (from to top to bottom: normal explicit, residual smoothing, semi-explicit, implicit operator splitting (Hujeirat & Rannacher 2001) and the fully implicit method). While the effective time covered in each run of these different methods is similar, the actual number of iteration is substantially different. The numerical problem here is to search stationary solutions for Taylor flow between two concentric spheres. The inner sphere has a radius  $r_{in} = 1$  and rotates with angular velocity  $\Omega_{in} = 5$ , whereas the outer sphere is non-rotating and its radius is taken to be  $r_{out} = 1.3$ .  $\theta = 1$  and  $\eta = 10^{-2}$  have been used in these calculations. The initial density and temperature are taken to be  $\rho(r, \theta, t=0) = 1$ , and  $T(r, \theta, t=0) = 10^1$ , respectively. The computational domain is  $[1, 1.3] \times [0, \pi/2]$  and consists of  $30 \times 50$  non-uniformly distributed tensor-product mesh.

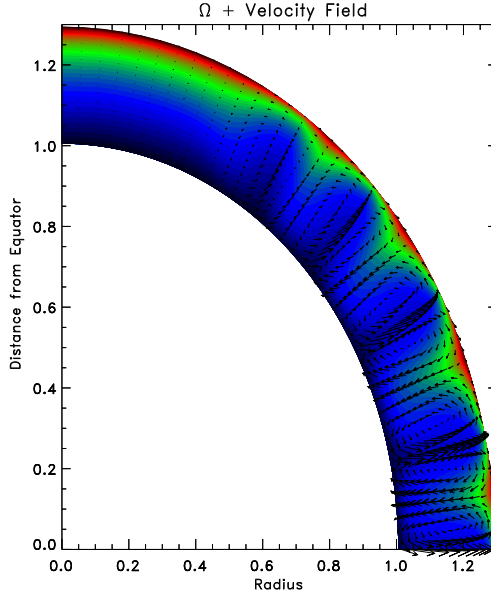


Fig. 14. Steady state solutions of the Taylor flow between two concentric spheres. Here the velocity field and the angular velocity (large-to-low values correspond to blue-to-red colors) are shown. The capability of the methods to capture the formation of rotationally-driven multiple vortices near-equatorial region is obvious.

level. Indeed, Fig. 15 shows that solving the angular momentum only may relax these limitations and that extremely large CFL-numbers can be obtained. 2) The conditions imposed on the boundaries are non-absorbing, and do not permit advection of errors into regions exterior to the domain of calculation. 3) The method requires probably additional improvements in order to achieve large CFL-numbers. This could be done, for example, within the context of the “defect-correction” iterative procedure, in which the block diagonal matrix  $D_{\text{mod}}$  is employed as a pre-conditioner.

In the final case (bottom, Fig. 13), the whole set of HD-equations is solved taking into account all pressure terms in a fully implicit manner. Here we use the AFM for solving the general block matrix-equation which is locally described by Eq. 18.

For controlling the time step size in these calculations, we have adopted the following description:  $\delta t = \alpha_0 \epsilon / \max(RHS_{j,k})$ , where  $\epsilon = \min(\Delta X_j, \Delta Y_k)$ , and where  $\alpha_0$  is a constant of order unity. The maximum and minimum functions here are set to run over the whole number of grid points.

Worth noting is the difference between the terminal values of the residual in the semi-explicit and the fully implicit cases. After a certain number of iteration, the residual in the former case does not decrease, and instead it shows strong, but still limited variations with increasing the number of iteration. Although a CFL-number of order 10 is achieved in this test calculations, the origin and magnitudes of these variations are not completely clear. However, taking into account that these strong variations do not show up in the fully implicit case, we may conclude that their origin is connected to the incomplete

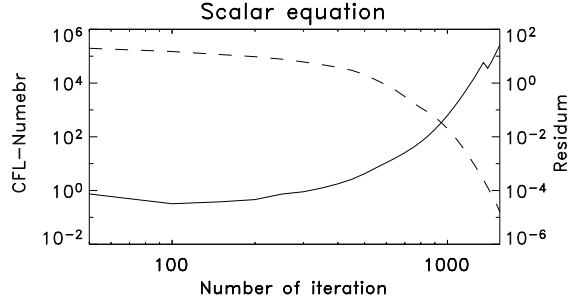


Fig. 15. The semi-explicit method applied to a scalar problem. As in Fig. 7, this Figure shows the development of the CFL-number (left axis, solid line) and the residual (right axis, dashed line) of the angular momentum equation in two dimensions versus the number of iteration. As initial conditions we use the steady distributions of the physical variables that have been obtained from the simulations of the Taylor problem (see Fig. 14). This includes the velocity field, density, temperature and  $\eta$ . For the angular velocity we use  $\Omega = 0$  as initial condition.

Table 1

The three different numerical approaches and their properties

	Explicit	Semi-Explicit	Implicit
Stability:	stable within $CFL < 1$	absolutely stable	absolutely stable
Convergence speed <sup>1</sup> :	limited by $CFL < 1$	faster than explicit, slower than implicit	unlimited by the CFL condition
Efficiency <sup>2</sup> :	highly efficient	efficient	inefficient
Robustness:	very limited	robust, but can be made highly robust <sup>3</sup>	robust
Programming efforts:	easy	easy	relatively difficult

inclusion of the source terms in the coefficient matrix.

## 6 Summary

In this paper a strategy for modifying explicit methods and constructing a class of semi-explicit methods is presented. We have shown that this modification enhance the robustness and enlarge the range of application of explicit methods, and in particular, it enables their use for searching quasi-stationary solutions for the Euler and Navier-Stokes equations in multi-dimensions.

The new strategy is based on reformulating explicit methods in matrix form, i.e, transforming explicit methods from scalar into matrix-vector problems. Thus, solving the set of time-dependent HD or MHD equations would require solving a matrix equation of the form:  $Aq = b$ . Explicit methods in this case relies on approximating and replacing the matrix  $A$  by the most simple matrix in algebra: the identity matrix  $I$ . This solution-procedure may converge, if the time step size is sufficiently small, or equivalently, if the entries of the matrix  $I/\delta t$  are sufficiently large, so that all off-diagonal elements of  $A$  can be safely neglected. As we have shown in Sec. 2, this yields a condition similar to the requirement that  $CFL < 1$ .

Unlike normal explicit methods, in which inclusion of diffusion generally causes further limitations on the time step size, diffusion operators in the semi-explicit formulation pronounce the diagonal dominance and enhances the stability of the inversion procedure, irrespective of the dimensionality of the problem. However, the convergence rates of semi-explicit methods remain lower than that of their fully implicit counterparts.

A relevant question which arises here is: how efficient are semi-explicit methods compared to explicit, and if they are more favorable than explicit methods when modelling time-dependent flows?

We note that in applying the semi-explicit method to a scalar equation, approximately  $N$  additional algebraic operations are required for calculating the diagonal elements, and roughly  $N$  division operations. Thus, applying the semi-explicit approach to system of equations of  $M$  variables, the additional algebraic operations required scale as:  $2 \times N \times M$ . If we take into account the addition global iterations required per each time step to assure convergence, we conclude that the semi-explicit methods are, indeed, less efficient than their explicit counterparts, provided the flow is strongly time-dependent. On the other hand, since the additional algebraic operations increases linearly with the total number of variables, the associated computational load is likely to be small compared to calculating the RHS of Eq. 7 or 16. Furthermore, the algorithm can be optimized further, in such a manner that the relevant routines, in which the corresponding additional operations are performed, are

---

<sup>1</sup> This applies for diffusion dominated flows, and within the regime of stability of the method. The discretization method used is assumed to be consistent/compatible with the continuous formulation. Semi-explicit methods converge relatively slowly, though not directly affected by the CFL-condition.

<sup>2</sup> A measure for the total computing operations per time step, provided the flow is time-dependent. This measure may reverse if the total number of computing operation is of interest, and if quasi-stationary solutions are sought.

<sup>3</sup> Reducing the semi-explicit method into explicit when modelling strongly time-dependent flows, and enhancing the degree of implicitness when modelling radiative, MHD and/or weakly/strongly incompressible flows through incorporating additional non-diagonal entries (see Fig. 1).

switched off if  $CFL < 1$ . In this case, the semi-explicit approach degenerates into an explicit method when the underlying flow is strongly time-dependent. This optimization procedure is particularly useful when modelling propagation of waves and moving shocks. The latter phenomena are non-linear features of HD-flows, and the corresponding equations do not admit stationary solutions. In this case, the time step size should be chosen sufficiently small in order to capture shock profiles accurately, irrespective of whether the method used is explicit or implicit. For modelling such flows, explicit methods are superior over implicit, provided that the flow is isothermal, adiabatic or polytropic. In the case that other physical and chemical processes are concerned, which generally operate on much shorter time scales than the dynamical time scale, modifying explicit methods into semi-explicit or strongly implicit is unavoidable.

In Table 1, the main properties of the new semi-explicit method, compared to explicit and implicit methods are listed.

Additionally, we have shown that the residual smoothing approach accelerates the convergence of both explicit and semi-explicit methods.

Acknowledgement: This research has been partially supported by SFB 359 “Reactive Strömungen, Diffusion und Transport” of the University of Heidelberg, Strasburg Observatory and the faculty of physics of Basel University. I thank the anonymous referee for her/his constructive and valuable suggestions, which improved the clarity and readability of the paper significantly.

## References

- [1] Balbus, S., Hawley, J., 1991,ApJ, 376
- [2] Beam, R.M., Warming, R.F., 1978, AIAA, 16, 393
- [3] Brandt, A., 2001,in Multigrid, ed.: Trottenberg, U., Oosterlee, C., Schüller, A., Acad. Press, London
- [4] Dongarra, I.S., Duff, D.C., Sorensen, H.A., van der Vorst, 1998, Num. Linear Alg. for High-Perormance Computers, SIAM
- [5] De Villiers, J.-P., & Hawley, J.F., 2003, ApJ, 589, 458
- [6] Enander, R., 1997, SIAM J. Sc. Comp., 18, 5, 1243
- [7] Fletcher, C.A.J., 1991, ”Computational Techniques for Fluid Dynamics”, Vol. I, II, 2nd Edition, Springer-Verlag
- [8] Font, J. A. 2000,Living Rev. Relativity, 3, 2

- [9] Fryxell, B., Olson, K., Ricker, P., et al., 2000, *ApJS*, 131, 273
- [10] Gammie, C.F., McKinney, J.C., Tóth, G., 2003, *ApJ*, 589, 444
- [11] Golub, G.H., Loan, C.F., 1989, "Matrix Computations", John Hopkins Univ. press, London
- [12] Hackbusch, W., 1994, "Iterative Solution of Large Sparse Systems of Equations", Springer-Verlag, New York-Berlin-Heidelberg
- [13] Hirsch, C., 1988, "Numerical Computation of Internal and External Flows", Vol. I, II, John Wiley & Sons
- [14] Hujerir, A., Rannacher, R., 2001, *New Ast. Reviews*, 45, 425
- [15] Kley, W., 1989, *A&A*, 208, 98
- [16] Koide, S., Shibata, K., & Kudoh, T. 1999, *ApJ*, 522, 727
- [17] Koide, S., Shibata, K., Kudoh, T., & Meier, D. L. 2002, *Science*, 195, 1688
- [18] Komissarov, S. S. 1999, *MNRAS*, 303, 343
- [19] Martí, J.M., & Müller, E., *LRR*, 2, 3
- [20] Meier, D.L., Koide, S., & Uchida, Y. 2001, *Science*, 291, 84
- [21] MacCormack, R.W., 1985, *AIAA*, Paper 85-0032
- [22] Richtmyer, R.D., Morton, K.W., 1967, "Difference methods for initial value problems", 2nd ed., Interscience, New York
- [23] Saad, Y., van der Vorst, 2000, *J. of Comp. and Appl. Math.*, 123, 1
- [24] Stone, J.M., Norman, M.L., 1992, *ApJS*, 80, 753
- [25] Swanson, R.C., Turkel, E., 1997, *NASA*, TP-3631, 81
- [26] Tóth, Keppens, R., Botchev, M.A., 1998, *A&A*, 332, 1159
- [27] Trottenberg, U., 2001, in *Multigrid*, ed.: Trottenberg, U., Oosterlee, C., Schüller, A., Acad. Press, London
- [28] Yabe, T., Xiao, F. Utsumi, T., 2001, *J. of Computational Physics*, 169, 556
- [29] Ziegler, U., 1998, *Comp. Phys. Comm.*, 109, 111

This figure "Fig5NA.jpg" is available in "jpg" format from:

<http://arxiv.org/ps/math-ph/0410054v1>

This figure "Fig7NA.jpg" is available in "jpg" format from:

<http://arxiv.org/ps/math-ph/0410054v1>

This figure "Fig8NA.jpg" is available in "jpg" format from:

<http://arxiv.org/ps/math-ph/0410054v1>

This figure "Fig11NA.jpg" is available in "jpg" format from:

<http://arxiv.org/ps/math-ph/0410054v1>